Research Article / Araştırma Makalesi GU J Sci, Part A, 9(2): 120-135 (2022) https://doi.org/10.54287/gujsa.1107158

Gazi University
Journal of Science
PART A: ENGINEERING AND INNOVATION
http://dergipark.org.tr/gujsa

Production and Characterization of Bilayer Tissue Scaffolds Prepared with Different Alginate-Salts and Fibroin

Özge ÇELİK[1], Salma A. Taher MOHAMED[2], Nuray EMİN[2,3*]

[1]*Kastamonu University, Engineering and Architecture Faculty, Genetic and Bioengineering Department, Kastamonu, 37150, Turkey*
[2]*Kastamonu University, Institute of Science and Technology, Material Science and Engineering Department, Kastamonu, 37150, Turkey*
[3]*Kastamonu University, Engineering and Architecture Faculty, Biomedical Engineering Department, Kastamonu, 37150, Turkey*

Keywords

Silk Fibroin
Alginate
Tissue Scaffold
Biomimetic Patch
Lyophilization

Abstract

The presented study aimed to design and characterize bilayer Alginate/Fibroin scaffolds to provide faster and higher quality treatment of skin tissue losses with tissue engineering approach. In this context, it was tried to form the dermis and epidermis layers with alginate salts (sodium and calcium) and fibroin with a biomimetic approach, and it was aimed to determine the most suitable alginate salt-fibroin composite scaffold by trying different production methods. The optimum design was determined by macroscopic measurement and dimensional analysis of the scaffolds produced by four different methods and their chemical structures were controlled with FTIR. Among the produced scaffolds, calcium alginate/fibroin (CaAlg/Fb) scaffolds were determined to have the most suitable morphological and chemical structure. With further characterization, the pore distribution and size were examined by SEM analysis and it was determined that surface pore diameters vary from 30 µm to 300 µm which are suitable for cell settlement. The thermal stability of the structure was determined by thermal gravimetry, and the degradation rate was calculated from the thermograms. According to the TG analysis, decomposition of the CaAlg/Fb scaffolds occurs much faster with temperature than homo-biopolymeric (CaAlg and Fb) structures. As a result, it was found that bilayer CaAlg/Fb scaffolds were capable of forming full-thickness dermal and/or also osteochondral wound dressings both morphologically and structurally. It is recommended to perform the tissue forming ability of this scaffold structure by performing advanced biological analyzes.

Cite

Çelik, Ö., Mohamed, S. A. T., & Emin, N. (2022). Production and Characterization of Bilayer Tissue Scaffolds Prepared with Different Alginate-Salts and Fibroin. *GU J Sci, Part A, 9*(2), 120-135.

Author ID (ORCID Number)

O. Çelik, 0000-0001-5186-0519
S. A. T. Mohamed, 0000-0002-6210-9920
N. Emin, 0000-0002-0859-2536

Article Process

Submission Date 21.04.2022
Revision Date 13.06.2022
Accepted Date 25.06.2022
Published Date 26.06.2022

1. INTRODUCTION

The skin consists of epidermis originated from ectoderm which is an epithelial lamina, dermis originated from mesoderm, which is a connective tissue lamina, and hypodermis. In addition, there are some supplements such as hair follicles, sweat and sebaceous glands, immune system cells and neural cells in the structure of the skin (Kanitakis, 2002; Woo, 2019). Damage to the skin occurs as a result of trauma, illness, burns and surgical procedures, and this can cause serious problems (Çakir & Yeğen, 2004). Burn trauma is one of the most common causes of major skin loss. As a result of thermal, chemical or electrical injuries, burns that are difficult to repair can occur on the skin (Summer et al., 2007; Toon et al., 2011). This causes contracture of the wound, scar tissue formation in the skin and loss of functional properties of the skin. All these negativities experienced in the ongoing routine treatment methods necessitated the search for a new treatment method. For this purpose, tissue engineering applications for regenerative treatment have gained importance (Priya et al., 2008; Chen & Liu, 2016). In this direction, various wound closure grafts have been designed, especially with the use of polymeric biomaterials, and the products that have been shown to be effective in experiments are patented under the name of therapeutic wound dressing (Reinholz et al., 2004; Yu et al., 2019). Skin conjugates

*Corresponding Author, e-mail: nurayemin@gmail.com

produced with the skin tissue engineering approach degrade while providing new tissue formation in the damaged area. Tissue-engineered wound dressings can consist of only three- or two-dimensional scaffolds, as well as contain isolated autologous cells and bio-signal molecules. Polymeric structures used in tissue engineering are produced from biocompatible natural or synthetic materials that can perform their functions by repairing tissues that cannot fulfil their functions or are used to support these tissues (Freed et al., 1994; Sittinger et al., 1996; Reinholz et al., 2004).

Silkworm silk has two different proteins. The first major protein is fibroin that gives silk its specific properties. The amino acid sequence of fibroin, which is hydrophobic, consists of 43% glycine, 30% alanine and 12% serine amino acids. Fibroin has been studied especially as a biomaterial for dermal patches, creating different designs, as it supports the adhesion and proliferation of the cells such as keratinocytes and fibroblasts (Ju et al., 2014). Sericin, which is the second major component of silkworm silk and holds fibroin together in the cocoons and constitutes 25-30% of the silk cocoon (Porter & Vollrath, 2009). Silk has widespread use in biomaterials applications thanks to its superior properties such as mechanical strength, good substance and gas permeability, biocompatibility, biodegradability and minimal inflammation (Hardy & Scheibel, 2010; Qi et al., 2017). It can be produced in the desired morphology (film, fiber, hydrogel and porous sponge) after being brought into solution (Vepari & Kaplan, 2007).

Alginic acid is a natural biopolymer isolated from red-brown seaweeds. It has a copolymer structure and consists of L-guluronic acid blocs and D-mannuronic acid blocs (Knill et al., 2004). Alginate has been proven to be non-toxic and biologically metabolized when taken orally. For this reason, it is used especially in pharmacological applications such as drug active ingredient, controlled released systems and tissue engineering. Alginate can be crosslinked with divalent metal cations to form hydrogel structure. For this purpose, calcium ions are often preferred (Peretz, 2004). Calcium alginate hydrogel is used in cell immobilization and encapsulation processes. Calcium alginate is used as a wound dressing in burn treatments because of its high biocompatibility and less pain (Kalia & Avérous, 2011).

The study aims to create a multi-layered wound dressing by using biopolymers with different properties by simulating the epidermis and dermis layers of the skin with a biomimetic approach. The epidermis is main lamina that is responsible for protection of the body against the both external influences and loss of substance from within the body. For this purpose, fibroin was preferred for the epidermis-mimicking surface, considering its good mechanical strength, more hydrophobic structure, antibacterial and wound healing properties (Clark et al., 2007; Hunt et al., 2009). The dermis is the main component of type I collagen. However, it is suggested that the use of collagen in the scaffold structure may be harmful in wound healing when the cells will be start producing their own collagen. However, animal-derived materials can promote the risk of immune rejection and disease infection (Clark et al., 2007). Therefore, there is a need for raw materials produced from non-animal sources for 2-layer dermal dressings. Because of that, alginate was chosen for the dermis-mimicking surface due to its water absorption ability, biocompatibility, faster biodegradation, and forming higher porose structure (Park et al., 2007; Hunt et al., 2009). While the alginate scaffold was produced in full thickness as a design, fibroin was applied in a thinner layer on the alginate scaffold, taking into account the layer thickness of the epidermis (MacNeil, 2007). The chemical structure of the produced 3D-tissue scaffolds was analyzed by FTIR, thermal properties were analyzed by Thermogravimetry (TG), the morphological structure was analyzed by Scanning Electron Microcopy (SEM) and the dimension analysis was analyzed by photographing. In order to give an idea about its biocompatibility, water holding capacity and biodegradability analyzes were performed for the scaffold structure, which was determined to be suitable.

2. MATERIAL AND METHOD

2.1. Preparation of Polymer Solutions

Two different natural polymers, silk fibroin and sodium alginate, were used in the preparation of composite tissue scaffolds. An aqueous solution of silk fibroin 3.64% and sodium alginate 3% (w/v) was used. The processing steps, which were carried out are described below.

2.1.1. Isolation and Purification of Fibroin

Silkworm cocoons were obtained from Bursa Koza Birlik (Türkiye). Fibroin was produced from silkworm cocoons using the standard alkaline method. Firstly, sericin in the Bombyx mori silkworm cocoons was removed by treatment in 500 ml of 0.02 M Na_2CO_3 (Sigma, USA) aqueous solution at boiling temperature for 30 minutes. Raw fibroin fibers were obtained and washed 2 times. Then, they were dissolved in 20,4 M LiBr (Sigma, USA) solution by incubation at 60°C for 3 hours. Then, it was taken into the dialysis membrane to purify it from salt and impurities, and it was dialyzed in distillated water for 3 days. Following the end of the dialysis process to remove the solid impurities, fibroin mixture was centrifuged at 4500 rpm for 20 minutes. The average solution concentration was calculated as 3.6% (w/v) by the gravimetric method.

2.1.2. Preparation of Sodium Alginate Solution

The alginate solution at the concentration of 3% (w/v) was prepared in 0.89% NaCl (Sigma, USA) solution. $CaCl_2$ solution was used as the crosslinker of sodium alginate. For this purpose, 0.4 M $CaCl_2$ (Sigma, USA) solution was prepared in 0.89% NaCl solution. All prepared solutions were stored at +4°C.

2.2. Scaffolds Fabrication

In the formation of tissue scaffolds as wound dressing, 4 different types of composite structures were created using the methods given in Table 1.

Table 1. *Composite structures planned to be formed and biopolymer mixing ratios*

No.	Scaffolding Composition	Fibroin Concentration (w/v %)	Alginate Concentration (w/v %)	Blend Ratio (v/v)
1	Na-Alginate/Fibroin	3,6	3	1:1
2	Na-Alginate/Fibroin-M (methanol applied)	3,6	3	1:1
3	Ca-Alginate/Fibroin	3,6	3	1:1
4	Ca-Alginate/Fibroin-M (methanol applied)	3,6	3	1:1

2.2.1. Preparation of the Sodium Alginate Scaffolds

Different methods were tried in the formation of composite scaffolds numbered 1 and 2 (NaAlg/Fb and NaAlg/Fb-M) which are given in Table 1, and optimum results were obtained by following the procedures given below.

- The polymer blend was prepared by mixing fibroin and sodium alginate at a 1:1 ratio by volume given in Table 1.
- After the polymer blend (NaAlg/Fb) was transferred to a 12-well petri dish, it was mixed gently.
- For the NaAlg/Fb-M scaffold, blend was prepared in the same way first. Then, 500 µl of methanol was added onto it.
- Polymer blends transferred to the mold were frozen at -24°C for 12 hours and at -86°C for 24 hours, respectively.
- After the first freezing process, the methanol-treated composite structures were washed with distilled water to remove excess methanol. Then, step 4 was repeated.
- The frozen polymer blends were placed in the lyophilizator and left to dry at -55°C for 24 hours.

2.2.2. Preparation of Calcium Alginate Scaffolds

Different methods were tried in the formation of composite scaffolds numbered 1 and 2 (CaAlg/Fb and CaAlg/Fb-M) which are given in Table 1, and optimum results were obtained by following the procedures given below.

- While forming the CaAlg/Fb and CaAlg/Fb-M composite scaffolds, firstly, CaAlg hydrogel was formed and then Fb coating was applied to it.
- For this, a 6-well petri dish was used as a mold and sodium alginate was added to each well.
- 0.4 M $CaCl_2$ was added to sodium alginate to form hydrogel by physical cross-linking.
- Fibroin solution was added so that the hydrogel was completely covered.
- CaAlg/Fb-M composite was prepared in the same way and 500 µl of methanol was added to it.
- Hydrogel-polymer composites were frozen at -24°C for 12 hours and at -86°C for 24 hours, respectively.
- After the first freezing process, the methanol-treated composite structures were washed with distilled water to remove excess methanol. Then, step 6 was repeated.
- The frozen polymer composites were placed in the lyophilization device and left to dry at -55°C for 24 hours.

2.3. Characterization of Composite Tissue Scaffolds

Macroscopic measurement and dimensional analysis of scaffolding structures were carried out metrically by photographing and the data were evaluated comparatively with each other. Bruker Alpha (USA) ATR-FTIR spectroscopy was used for the structural analysis of composite dressing materials. Measurements were carried out at a scanning speed of 4 cm^{-1} in the range of 400-4000 cm^{-1}. Further characterization was continued with the CaAlg/Fb sample, which was determined to have surface properties that could be used as a wound dressing according to the results of macroscopic size and morphology analysis and FTIR analysis. The FEI Quanta FEG 250 (USA) The surface morphology of the composite wound dressing materials was analyzed using Scanning Electron Microscopy (SEM). Thermal degradation changes were tested with Hitachi STA7300 (Japan) Thermal analyzer in a nitrogen atmosphere between 25°C-800°C.

According to the characterization analysis results, the water uptake capacity of the CaAlg/Fb scaffold, which was determined to have sufficient properties was calculated gravimetrically by keeping it in distilled water at 37°C for 24 hours. In addition, the pH change was monitored for 24 h by taking hourly measurements for first 6 hours.

3. RESULTS AND DISCUSSION

3.1. Macroscopic Measurements

Macroscopic measurement and dimensional analysis were performed by photographing against a metric scale. First of all, it was tried to determine the most suitable method in macroscopic morphology for the scaffolds produced with 2 different methods according to Table-1 in the study program. It was determined that the structural integrity of the NaAlg/Fb scaffolds was more preserved than the NaAlg/Fb-M structure. It was measured that NaAlg/Fb scaffolds had a diameter of approximately 2.0 cm and a diameter of approximately 2.3 cm for NaAlg/Fb-M scaffolds (Figure 1A-B). Although the samples treated with methanol had a larger diameter, it was observed that the surface morphology and scaffold thickness did not conform to expectations. Similar results were obtained for CaAlg/Fb and NaAlg/Fb scaffolds. It was determined that among all scaffold samples, CaAlg/Fb scaffolds had the most suitable structure in terms of structural integrity and surface homogeneity and thickness. Dimensionally, CaAlg/Fb scaffolds have a diameter of 2.5 cm, and CaAlg/Fb-M scaffolds have a diameter of around 2 cm (Figure 1C-D). In addition, in CaAlg/Fb-M samples, it was determined that the fibroin layer was not sufficiently integrated into the alginate surface and separated from the surface after methanol treatment.

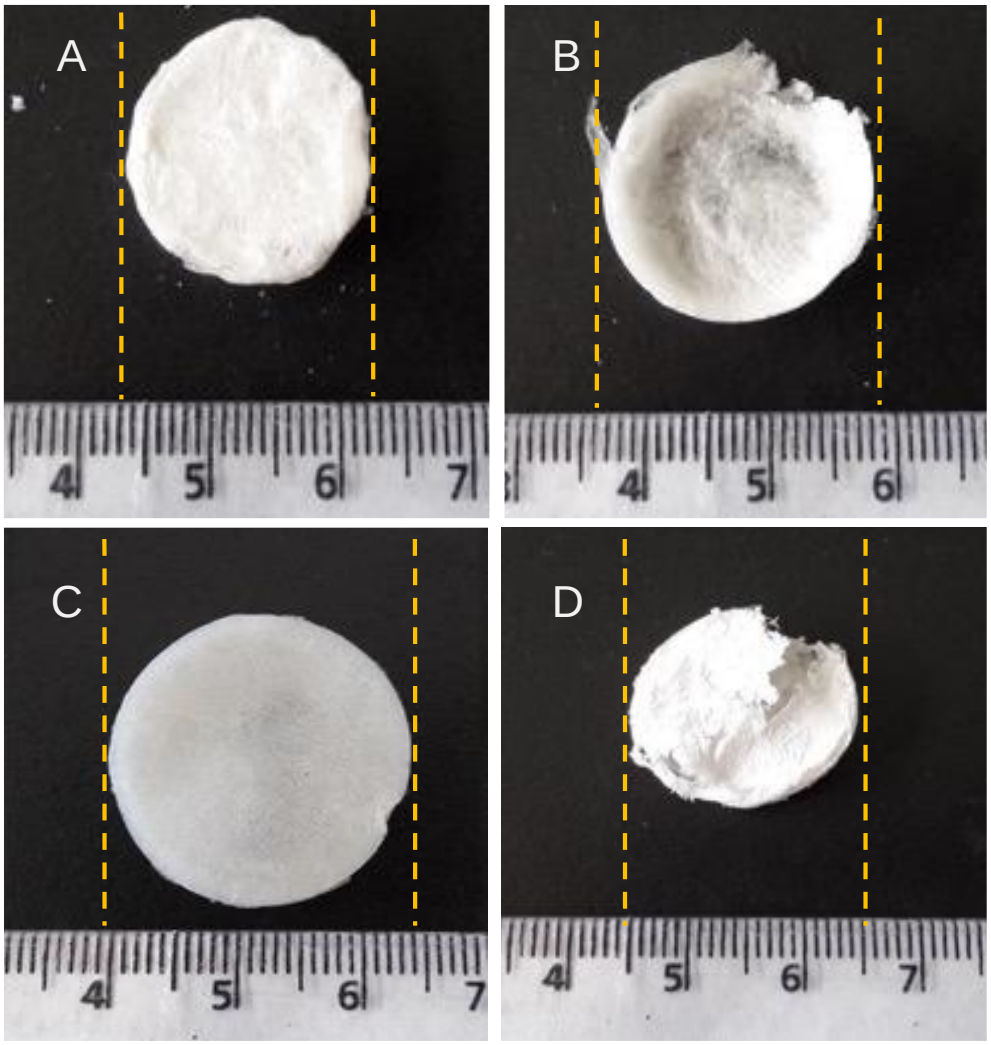

Figure 1. *Macroscopic dimension evaluation of composite scaffolds;*
A) *Na-Alg/Fb,* ***B)*** *Na-Alg/Fb-M treated with methanol,* ***C)*** *CaAlg/Fb,* ***D)*** *NaAlg/Fb-M treated with methanol*

The use of methanol reduces its degradation in aqueous media by supporting the β-layer structure and increasing the interaction between the layers (Qi et al., 2017; Zhao et al., 2021). Studies have shown that organic solvents disrupt the β-layer structure of fibroin, causing irregular pore structure in a mono-alcohol-treated fibroin scaffolds (Zhang et al., 2021). In this respect, the literature findings are consistent with our results and support that the shape distortions in all methanol-treated scaffold samples are due to the effect of methanol on amide bonds.

3.2. Chemical Structure Properties of Composite Tissue Scaffolds

FT-IR spectra for the structural analysis of the obtained scaffolds are given in Figure 2. The stretching vibrations of the O–H bonds of the alginate were observed in the range of 3000-3600. Aliphatic C–H stretching vibrations were observed at 2920-2850 cm^{-1}. The bands observed at 1597 and 1411 cm^{-1} in NaAlg, 1604 cm^{-1} and 1420 cm^{-1} in CaAlg show the asymmetric and symmetric stretching vibrations of the carboxylate salt ion, respectively. These alginate-specific peaks were observed at a higher wavenumber in the calcium salt structure compared to the sodium salt. Subsequent bands are very important and can be used to characterize the alginate from the blends and derivatives. The bands at 1107 and 935 cm^{-1} were evaluated as C–O stretching with contributions from the C–O stretching vibration of the pyranose rings and the C–O–H and C–C–H deformation. Symmetric and asymmetric tensile bands belonging to the C–O–C group were found at 1087 cm^{-1} and 1028 cm^{-1} respectively. In CaAlg, it was observed that the peaks in this range expanded and new peaks of weak intensity were formed. This is due to the chelate structures formed by Ca and gluronic acid in the pyran ring structure.

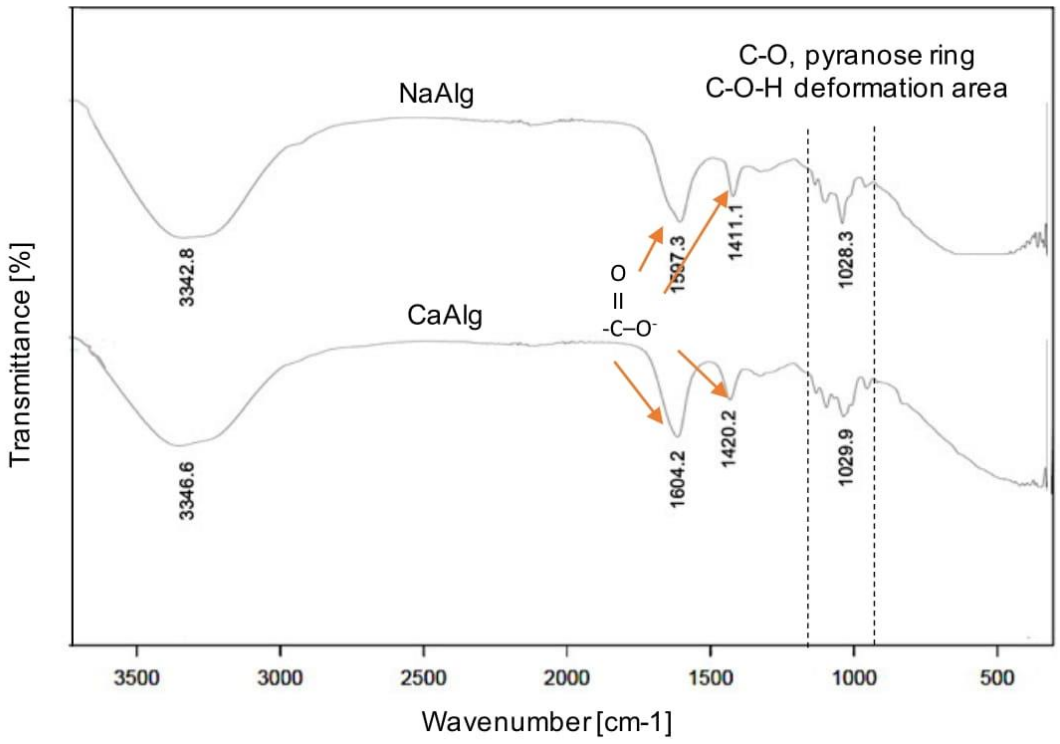

Figure 2. *FTIR spectrum of Na-Alginate and Ca-Alginate*

When the FTIR spectra of Na-Alg/Fb and NaAlg/Fb-M scaffolds were compared; Before treatment with methanol, the characteristic bands of amide I and amide II in silk-I structure, were observed at 1621 cm^{-1} (amide I), 1519 cm^{-1} (amide II), respectively. It has been observed that the -NH stresses are in the region of 3279 cm^{-1}. After the treatment with methanol, it is seen that these bands shifted to 1620 cm^{-1} and 1518 cm^{-1}, respectively, and the peak intensity increased (Figure 3). This proves that the transition to the β-layer structure has been achieved (Amiraliyan et al., 2010). Furthermore, as it can be seen in (Figure3), there is a small split doublet between band values 1620 cm^{-1} and 1518 cm^{-1}, indicating conformation from random coil to β-sheet. The results showed that the use of methanol has resulted in the conformation to β-sheet structure (Zhang & Mo, 2011; Shen et al., 2022; Xie et al., 2022).

In the FTIR spectra of silk fibroin and composites stabilized by methanol treatment, amide bands are examined in the range of 1700 cm^{-1}-1500 cm^{-1}. Amid I covers the range of 1700 cm^{-1}-1600 cm^{-1}, and amide II covers the range of 1600 cm^{-1}-1500cm^{-1} (Jaramillo-Quiceno et al., 2017). The 1610-1630, 1695-1700 and 1510-1520 cm^{-1} peaks are the characteristic absorption peaks for the secondary structure silk-II conformation (Bhattacharjee et al., 2013). Absorption peaks of 1648-1654 cm^{-1} and 1535-1542 cm^{-1} are characteristic pics of the amorphous silk-I conformation (Hu et al., 2006; Lu et al., 2011).

In the FTIR graph of the fibroin scaffold, the stretching vibrations of the –OH bonds were seen at 3279 cm^{-1} and between 3600-3200 cm^{-1} area. Stretching vibrations of aliphatic -C-H were observed between 3065 cm^{-1} and 2935 cm^{-1} peaks. Amid I bond shows C=O stretching at 1621cm^{-1}; Amid II bond shows N–H bending at 1519 cm^{-1}; Amid III bond shows C–N stretching at 1233 cm^{-1} were observed (Bhattacharjee et al., 2013). The beta-layer structure of fibroin, which is composed of antiparallel polypeptide chains, is rich in glycine and generally contains chains formed by repeating the Gly-Ser-Gly-Ala_Gly_Ala sequence. In addition, small amounts of amino acids with large side chains such as Tyr, Val, Arg and Asp are also present in the structure. These cause the structure to deviate from the crystalline order (Nelson & Cox, 2008/2013; Pamuk, 2011). In our study, peaks of fibroin-specific gly-gly and gly-ala petit motifs were observed in the 1000 and 970 cm^{-1} area. These bonds and functional groups are specific to the protein structure of fibroin. It is seen that the chemical structure of fibroin is preserved in the experimental stages.

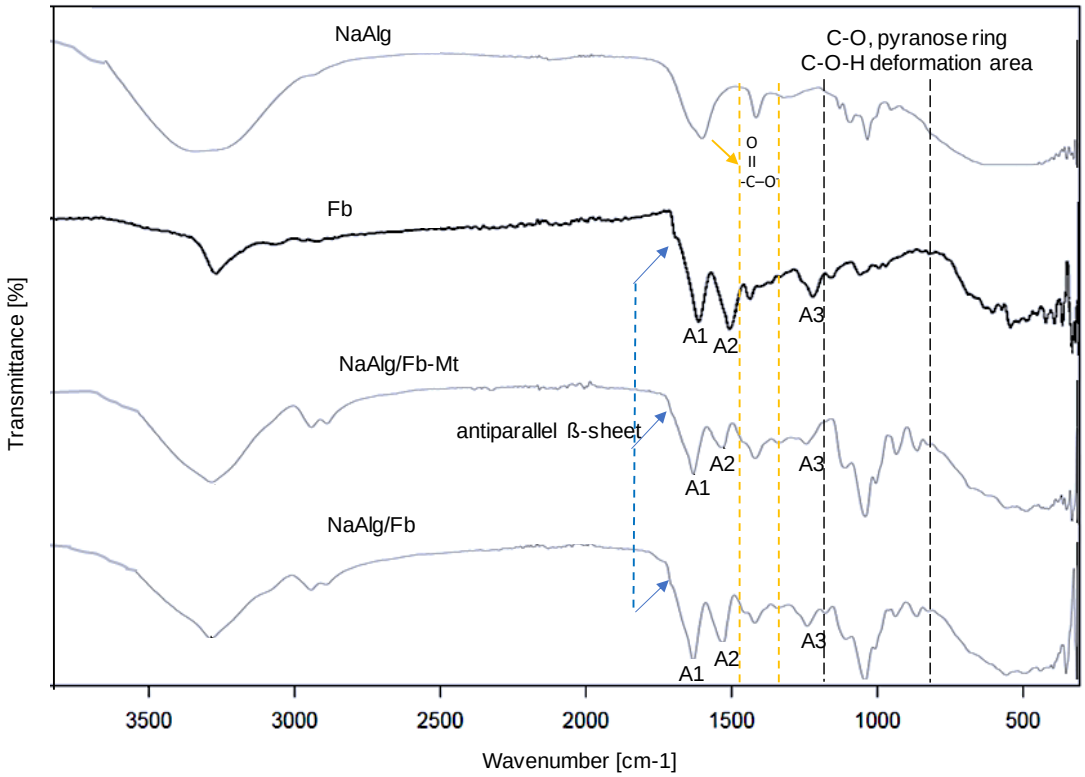

Figure 3. *FTIR spectra of NaAlg, NaAlg/Fb, Silk Fibroin (Fb), and NaAlg/Fb-M*
A1: *Amide I,* ***A2:*** *Amide II,* ***A3:*** *Amide III*

Bhattacharjee et al. (2013) detected tensile bands at 1622, 1506 and 1227 cm^{-1} for Amid I, II and III, respectively, for the 3D silk fibroin sample. It has been reported that shifting of these bands is expected in the treated samples. In this study, the measured values for amide bonds of fibroin were obtained at 1621, 1519 and 1233 cm^{-1} in accordance of the literature (Bhattacharjee et al., 2013; Hofmann et al., 2014; Shen et al., 2022; Xie et al., 2022). In addition, it was determined that these values showed a shift according to the applied scaffolding production methods and composite composition (Xie et al., 2022).

The characteristic peaks representing the protein structure of fibroin in the CaAlg/Fb and CaAlg/Fb-M scaffolds are caused by the stretching of the amide I and amide II bonds and are 1635 cm^{-1}, 1515 cm^{-1} for CaAlg/Fb, and 1621 cm^{-1}, 1516 cm^{-1} for CaAlg/Fb-M, respectively. These are the peaks at wavenumbers of 1621 cm^{-1} and 1516 cm^{-1}. By comparing the spectra of both structures, the presence of fibroin in CaAlg/Fb was determined qualitatively (Figure 4).

Silkworm silk fibroin can be found in its secondary structure in two basic conformations, silk I and silk II. Although the structure of the Silk I conformation is not fully understood, it is known to be a mixture of α-helix and random helical structures. This metastable nature of silk fibroin is not a desirable conformation for many applications due to its water solubility. Instead, silk II structured materials containing anti-parallel β-layers are preferred. Alcohols like that ethanol and methanol can be used for crystallization of the silk fibroin molecules (Bhattacharjee et al., 2013; Hofmann et al., 2014; Shen et al., 2022). It is thought that the crystallization mechanism is primarily in the form of the interaction of the polar alcohol, which can form hydrogen bonds, with the water in the environment, and as a result, hydrophobic amino acids such as alanine and glycine cluster to form the planar β-layer structure. Amide bond concentration increase was also observed in methanol treatment samples with increasing physically cross-linking between chains (Um et al., 2001).

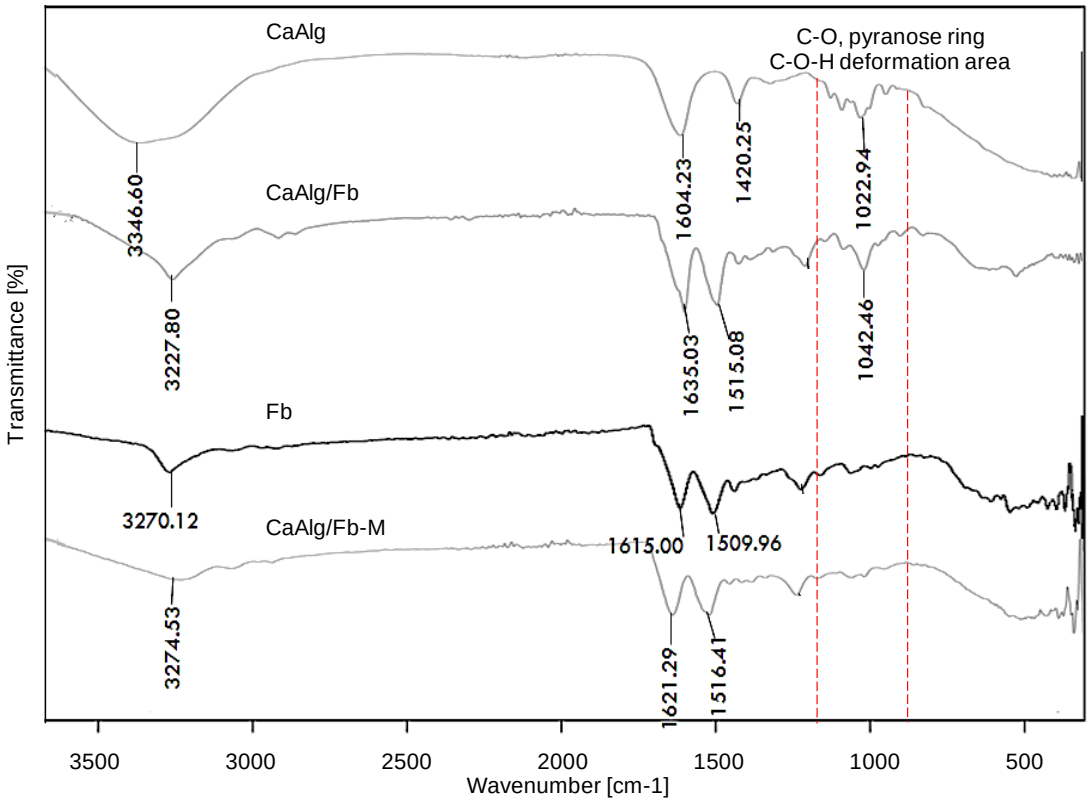

Figure 4. *FTIR spectra of CaAlg, CaAlg/Fb, Silk Fibroin (Fb), and CaAlg/Fb-M*

3.3. Evaluation of Surface Morphology

SEM images were taken to examine the structure of the composite tissue scaffolds and to determine the pore diameters (Figure 5). In the SEM image of the scaffold produced by lyophilization using only fibroin (Figure 5C), layered structures are remarkable. On the other hand, it is seen that the scaffold produced under the same conditions using calcium alginate has a more porous structure. The layered parts seen in the SEM micrographs of the CaAlg/Fb composite scaffold in Figure 5A-B are fibroin. When the overall SEM image of the composite scaffold at 100x magnification is examined, it is seen that the scaffold has a porous structure. In addition, there is no sign of damage or impairment, meaning that the integrity of the whole scaffold remained intact. Consequently, porous scaffolds, which are three-dimensional polymeric scaffolds with increased porosities and a homogenous interconnected pore network, are very advantageous in tissue engineering practices (Loh & Choong, 2013). The porous structure can be seen more clearly in SEM micrographs at 250x magnification at Figure 5B. It is seen that the pores in the structure are interconnected and have an open pore structure. Moreover, it is seen that the pore distribution showed homogeneous patterning, and the surface pore diameters vary from 30-70 µm to 300 µm. It has been determined that the pore diameters of the composite scaffold are suitable for the placement of the cells. However, it is seen that the pores with diameters in the range of 35-140 µm are more in the structure. In tissue engineering applications for wound dressings, porosity in the range of 20-125 µm is reported to be ideal for growth and regeneration of skin tissue (Xie et al., 2022). In this respect, it can be said that the pore structure of CaAlg/Fb scaffolds is suitable for skin tissue engineering.

Although direct mixing was not applied to the polymers it was determined that fibroin interacted with Ca-Alginate and thus its layered structure was disrupted and its porosity increased (Xie et al., 2022). Shen et al. (2022), in their study in which they examined the effects of sodium alginate nanoparticle uses on silk fibroin-sodium alginate scaffolds, SEM images of fibroin-alginate scaffolds prepared by lyophilization are similar to our samples in terms of porosity (Shen et al., 2022). The literature supports that the layered areas in the CaAlg/Fb composite structure originate from fibroin. This morphological feature is of great significance as implant location and 3D tissue development are influenced by the scaffold's porous nature and porosity. Pores are necessary for tissue creation because they allow for cell migration and proliferation, as well as vascularization and nutrition transport (Griffon et al., 2006; Xie et al., 2022).

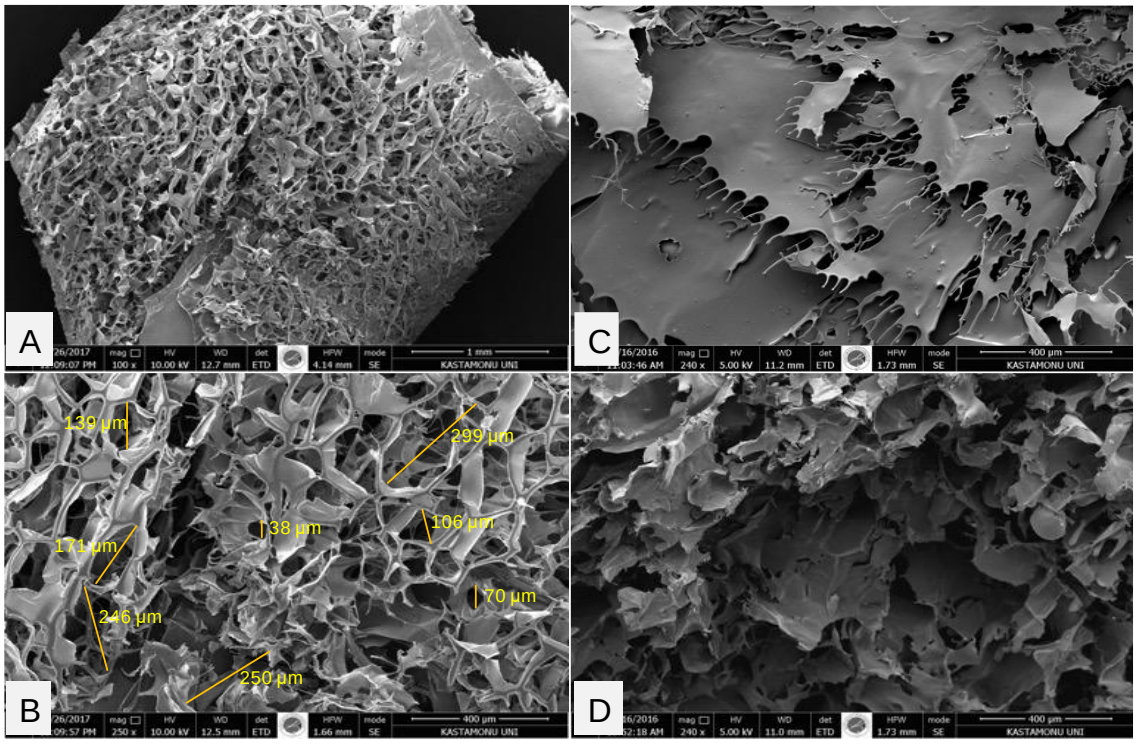

Figure 5. *SEM images of scaffolds;*
A)*100x and* ***B)*** *250x magnified view of CaAlg/Fb composite scaffold,* ***C)*** *fibroin and* ***D)*** *alginate scaffold*

3.4. TGA Analysis

It is conventional knowledge that finding materials with better properties for a specific application requires a comprehensive understanding of polymer degradation characteristics when heated (Coats & Redfern, 1963). Thermal Analysis is a method in which the physical and chemical properties of materials are examined depending on temperature. Temperature change causes several chemical and physical effects such as evaporation of the structural water, desorption, degradation reactions etc. on the material. TGA analysis was preferred to determine the relationship between the change in mass of fibroin scaffolds and temperature. Thermograms of composite scaffolds and homopolymeric structures (CaAlg and Fb) are given in Figure 6. In these thermograms, it was determined that the chemical structure of calcium alginate underwent thermal degradation at five points (105.2°C, 151.4°C, 265.8°C, 421.9°C, 505.1°C) in the range of 25-800°C. It was observed that the chemical structure of pure fibroin underwent thermal degradation at three points (37.2°C, 255.6°C, 609.3°C) in the same temperature range. In the CaAlg/Fb scaffold sample, on the other hand, it was determined that the chemical structure occurred as thermal decomposition at only four points (230.9°C, 419.5°C, 505.8°C, 631.3°C). In CaAlg/Fb composite scaffolds, the increase in thermal stability of the structure and the occurring degradation at different temperatures than the pure biopolymeric structures showed that first hydrogelation of sodium alginate with Ca^{2+} ions and then treatment with fibroin solution provided better integration amongst biopolymers. This would mean that the thermal stability of the composite scaffolds has been improved in a clear manner, as a consequence of the decelerated disintegration rate, a higher heating rate gave greater thermal stability (Coats & Redfern, 1963).

The mass changes of CaAlg/Fb and homopolymeric structures on the decomposition temperatures in the thermograms were calculated as a percentage of degradation for all samples and are given in Table 2. Although the thermal degradation stability of CaAlg/Fb scaffolds increased, the rate of degradation by mass decreased only in the range of 151-266°C compared to biopolymeric structures.

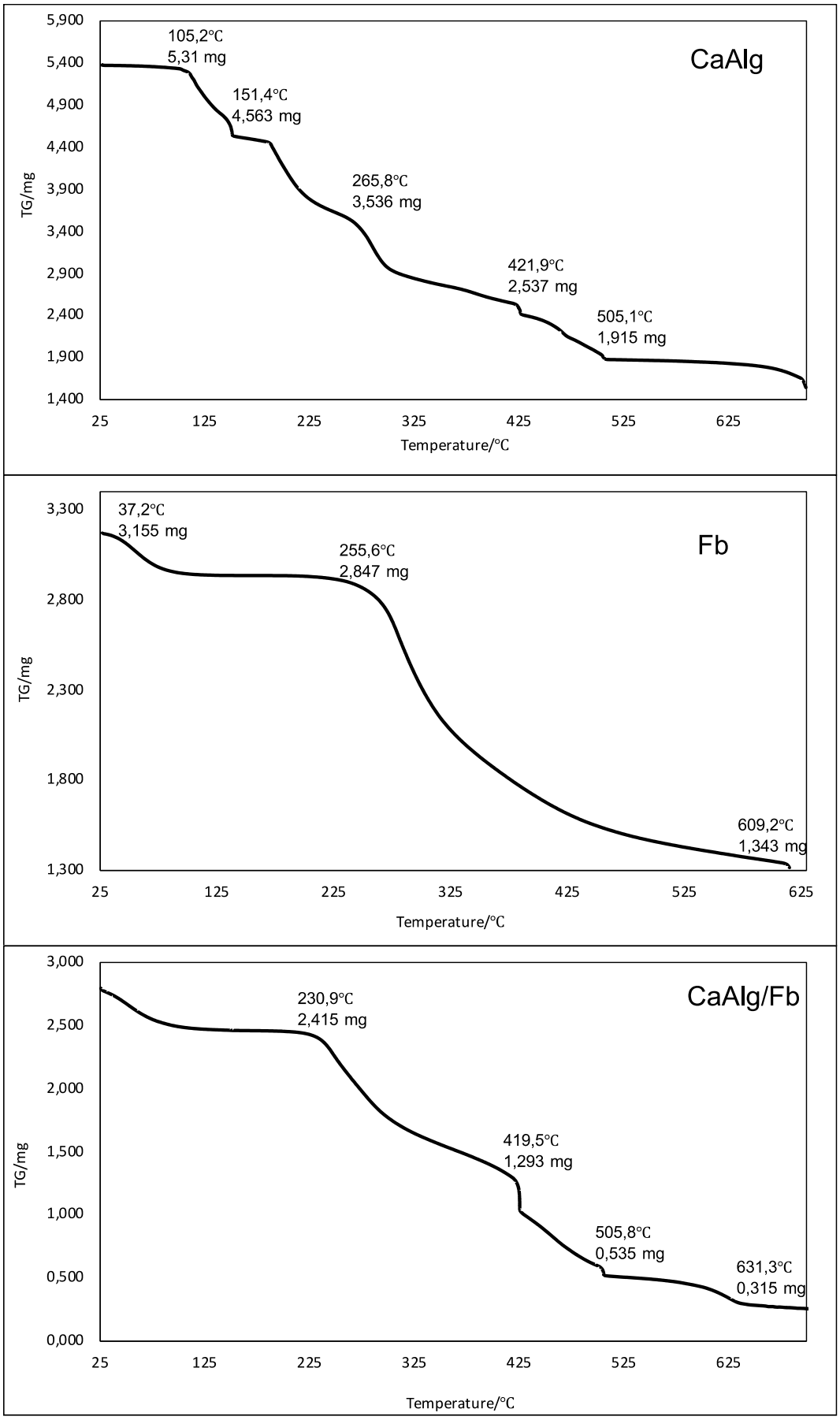

Figure 6. *TG thermograms of the CaAlg, Fb and CaAlg/Fb*

Table 2. *Thermal degradation rates of CaAlg, Fb and CaAlg/Fb samples*

TEMPERATURE (°C)	DEGRADATION RATIO (%)		
	CaAlg	Fb	CaAlg/Fb
37,16	0,13	0,65	2,09
105,18	1,24	7,27	11,25
151,40	15,29	7,48	12,12
230,85	30,51	8,29	13,88
255,57	33,17	10,36	22,11
265,80	34,47	12,28	25,97
419,49	52,69	48,56	53,89
421,90	52,90	48,81	54,70
505,10	64,45	54,18	80,05
505,82	64,70	54,21	80,91
609,83	65,73	57,73	85,62
631,30	66,03	58,67	88,75

The some physical, chemical and mechanical properties of fibroin can be changed in the presence of various crosslinkers or by the use of thermal processes (Rujiravanit et al., 2003; Mirahmadi et al., 2013; Ghezzi et al., 2014; Yodmuang et al., 2015). For example, water solubility, durability and porous structure formation can be changed by changing thermal processes or by using chemical reagents such as methyl alcohol and glutaraldehyde (Wang et al., 2015). Evaluation of the TG findings, it has been determined that the decomposition of the structure occurs much faster with temperature than in homo-biopolymeric structures. In the fibroin molecule, there are many hydrogen bonds within and between the chains. This might be attributed to the reason that neighboring chains are kept together in an anti-parallel configuration by strong hydrogen bonds to form (β-sheets) and as a result, the fibroin's strength is substantially reinforced (Cheng et al., 2014). For this reason, fibroin is resistant to thermal degradation and to acids and bases due to its amphoteric properties. On the other hand, significant shifts were determined in the thermal degradation of fibroin in the composite structure. This shows that CaAlg reduces intramolecular secondary interactions in the structure of fibroin and thus, increases its thermal degradation.

3.5. Water Uptake Capacity and pH Changes

The ability of a biomaterial to retain water is an indicator for its biocompatibility. Materials that can easily absorb water also facilitate the adhesion of cells to the surface (Hu et al., 2021). The water holding capacity of CaAlg/Fb scaffolds, which were determined to have sufficient properties as a result of physical and chemical characterization analyzes, was tested. The treatments were carried out in distilled water under physiological temperature conditions in 3 repetitions. The results obtained are given in Table 3, and it was determined that the composite scaffold could absorb water up to 211.07% of its dry weight.

Table 3. *Water uptake capacity of the CaAlg/Fb*

Sample	Average Water Uptake (%)	Standard Derivation
CaAlg/Fb	211,07	22,72

When a scaffold is taken into cell culture, daily or every other day media change is performed considering its biodegradability and tissue development. Therefore, how the CaAlg/fb scaffold changed the physiological pH conditions of HANK's balanced medium was followed for 24 hours using a pH-meter. The first 6 hours of the experiment were measured hourly. The results are given in Figure 7. The pH change in the first 6 hours was close to linear, and then it remained horizontal. At the end of 24 hours, the pH was measured as 7.83. The pH change remained within the range where the skin cells could maintain their vital functions.

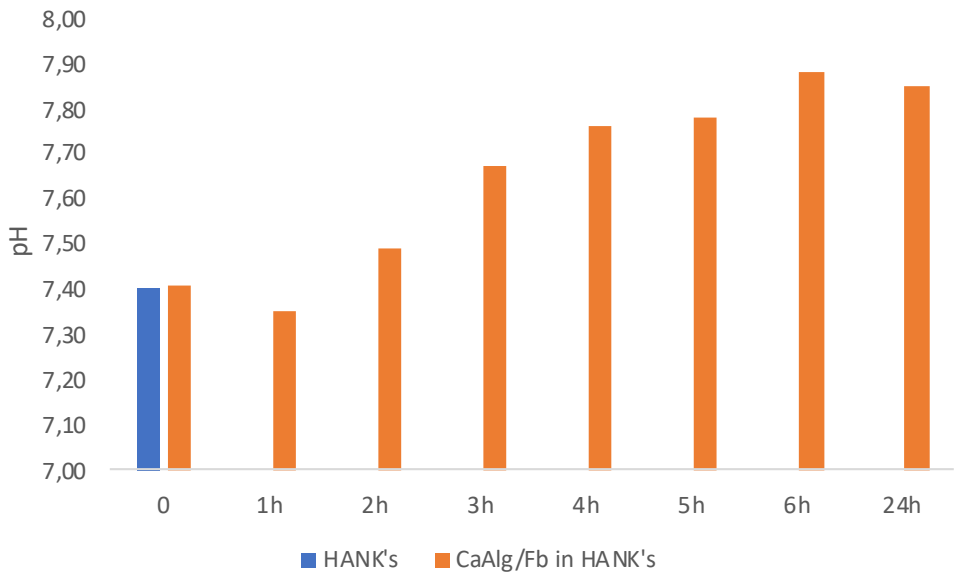

Figure 7. *pH changes of the culture media with CaAlg/Fb scaffold*

4. CONCLUSION

Within the scope of the study, which was carried out using the sodium salt of alginic acid, four different scaffold structures were obtained that can be used in dermal wounds. The design of the scaffolds was made by considering the dermis and epidermis for dressing use. Within the scope of the study, which was carried out using the salts of alginic acid, four different scaffold structures were obtained that can be used in dermal wounds. The design of the scaffolds was made by considering the dermis and epidermis for dressing use. For the dermis structure, alginic acid was preferred in accordance with the literature, taking into account its mechanical and chemical properties (Park et al., 2007; Hunt et al., 2009). Considering the more stable structure and natural wound healing properties of fibroin and its routine use, it was preferred for the epidermis layer. Our evaluations were also conducted considering its usability as a two-layer full-thickness dressing. While sodium alginate-fibroin scaffolds were formed by mixing fibroin and sodium alginate solutions, calcium alginate-fibroin scaffolds were obtained by coating calcium alginate hydrogel with fibroin solution. It showed that alginate derivatives and fibroin were integrated to each other at certain rates in all scaffold structures.

FTIR results showed that fibroin chains were rearranged by the interaction of fibroin with methanol. In this way, it is understood that there is a transformation of the crystalline β-layer structure. However, these rearrangements of fibroin chains themselves reduced the affinity of fibroin to alginate. As a result, although an obvious interface was formed at the border between the polymer surfaces, it was determined that fibroin was separated from the alginate surface and its macroscopic morphology lost its homogeneity. According to the dimensional and chemical analysis of the produced scaffolds, the best results were obtained in CaAlg/Fb samples obtained by hydrogelation of calcium alginate and then coating with fibroin solution (Figure 8). For this reason, further characterization was carried out on this scaffold sample.

With CaAlg/Fb scaffolds, bi-layer and full-thickness scaffolds with morphology which can be used as dermal wound dressing were obtained. Although these scaffolds were not mixed together in solution, it was clearly seen in the SEM and TG analysis that the penetration of the fibroin solution into the calcium alginate hydrogel took place. It has been determined that the chemical structure deterioration of calcium alginate, which starts at lower temperatures, decreases in the composite structure and occurs at higher temperatures. On the other hand, it has been determined that the rate of thermal degradation occurs at a near linear rate in scaffold structures and in a more controlled manner than homo-polymeric structures. As a result, a bi-layer wound dressing like scaffold, compatible with the anatomical and histological structure of the dermis and epidermis, was obtained using by alginate and fibroin respectively. In these processes, it has been shown that the use of alginic acid, a block copolymer with polyanion structure, in hydrogel form increases the stability of the structure and can be physically cross-linked with amphoteric fibroin using hydrogen bonds and dipole interactions.

Figure 8. *CaAlg/Fb scaffold*

ACKNOWLEDGEMENT

This study was partially supported by Kastamonu University BAP Office with the KÜBAP 2015-27 research project number. The authors would like to thank Kastamonu University Central Research Laboratory Research and Application Center for the infrastructure support they provided in the realization of the study.

CONFLICT OF INTEREST

This study was conducted as a postgraduate study under the supervision of Nuray Emin. The authors declare no conflict of interest.

REFERENCES

Amiraliyan, N., Nouri, M., & Haghighat Kish, M. (2010). Structural characterization and mechanical properties of electrospun silk fibroin nanofiber mats. *Polymer Science Series A*, *52*(4), 407-412. doi:10.1134/S0965545X10040097

Bhattacharjee, M., Schultz-Thater, E., Trella, E., Miot, S., Das, S., Loparic, M., Ray, A. R., Martin, I., Spagnoli, G. C., & Ghosh, S. (2013). The role of 3D structure and protein conformation on the innate and adaptive immune responses to silk-based biomaterials. *Biomaterials*, *34*(33), 8161-8171. doi:10.1016/j.biomaterials.2013.07.018

Chen, F.-M., & Liu, X. (2016). Advancing biomaterials of human origin for tissue engineering. *Progress in Polymer Science*, *53*, 86-168. doi:10.1016/j.progpolymsci.2015.02.004

Cheng, Y., Koh, L.-D., Li, D., Ji, B., Han, M.-Y., & Zhang, Y.-W. (2014). On the strength of β-sheet crystallites of Bombyx mori silk fibroin. *Journal of the Royal Society Interface*, *11*(96), 20140305. doi:10.1098/rsif.2014.0305

Clark, R. A. F., Ghosh, K., & Tonnesen, M. G. (2007). Tissue engineering for cutaneous wounds. *Journal of Investigative Dermatology*, *127*(5), 1018-1029. doi:10.1038/sj.jid.5700715

Coats, A. W., & Redfern, J. P. (1963). Thermogravimetric analysis. A review. *Analyst*, *88*(1053), 906-924. doi:10.1039/AN9638800906

Çakir, B., & Yeğen, B. Ç. (2004). Systemic responses to burn injury. *Turkish Journal of Medical Sciences*, *34*(4), 215-226.

Freed, L. E., Marquis, J. C., Langer, R., Vunjak-Novakovic, G., & Emmanual, J. (1994). Composition of cell-polymer cartilage implants. *Biotechnology and Bioengineering*, *43*(7), 605-614. doi:10.1002/bit.260430710

Ghezzi, C. E., Marelli, B., Donelli, I., Alessandrino, A., Freddi, G., & Nazhat, S. N. (2014). The role of physiological mechanical cues on mesenchymal stem cell differentiation in an airway tract-like dense collagen–silk fibroin construct. *Biomaterials*, *35*(24), 6236-6247. doi:10.1016/j.biomaterials.2014.04.040

Griffon, D. J., Sedighi, M. R., Schaeffer, D. V., Eurell, J. A., & Johnson, A. L. (2006). Chitosan scaffolds: interconnective pore size and cartilage engineering. *Acta Biomaterialia*, *2*(3), 313-320. doi:10.1016/j.actbio.2005.12.007

Hardy, J. G., & Scheibel, T. R. (2010). Composite materials based on silk proteins. *Progress in Polymer Science*, *35*(9), 1093-1115. doi:10.1016/j.progpolymsci.2010.04.005

Hofmann, S., Stok, K. S., Kohler, T., Meinel, A. J., & Müller, R. (2014). Effect of sterilization on structural and material properties of 3-D silk fibroin scaffolds. *Acta Biomaterialia*, *10*(1), 308-317. doi:10.1016/j.actbio.2013.08.035

Hu, K., Hu, M., Xiao, Y., Cui, Y., Yan, J., Yang, G., Zhang, F., Lin, G., Yi, H., Han, L., Li, L., Wei, Y., & Cui, F. (2021). Preparation recombination human-like collagen/fibroin scaffold and promoting the cell compatibility with osteoblasts. *Journal of Biomedical Materials Research Part A*, *109*(3), 346-353. doi:10.1002/jbm.a.37027

Hu, X., Kaplan, D., & Cebe, P. (2006). Determining beta-sheet crystallinity in fibrous proteins by thermal analysis and infrared spectroscopy. *Macromolecules*, *39*(18), 6161-6170. doi:10.1021/ma0610109

Hunt, N. C., Shelton, R. M., & Grover, L. (2009). An alginate hydrogel matrix for the localised delivery of a fibroblast/keratinocyte co-culture. *Biotechnology Journal*, *4*(5), 730-737. doi:10.1002/biot.200800292

Jaramillo-Quiceno, N., Álvarez-López, C., & Restrepo-Osorio, A. (2017). Structural and thermal properties of silk fibroin films obtained from cocoon and waste silk fibers as raw materials. *Procedia Engineering*, *200*, 384-388. doi:10.1016/j.proeng.2017.07.054

Ju, H. W., Lee, O. J., Moon, B. M., Sheikh, F. A., Lee, J. M., Kim, J.-H., Park, H. J., Kim, D. W., Lee, M. C., Kim, S. H., Park, C. H., & Lee, H. R. (2014). Silk fibroin based hydrogel for regeneration of burn induced wounds. *Tissue Engineering and Regenerative Medicine*, *11*(3), 203-210. doi:10.1007/s13770-014-0010-2

Kalia, S., & Avérous, L. (2011). *Biopolymers: biomedical and environmental applications* (Vol. 70). John Wiley & Sons.

Kanitakis, J. (2002). Anatomy, histology and immunohistochemistry of normal human skin. *European Journal of Dermatology*, *12*(4), 390-401.

Knill, C. J., Kennedy, J. F., Mistry, J., Miraftab, M., Smart, G., Groocock, M. R., & Williams, H. J. (2004). Alginate fibres modified with unhydrolysed and hydrolysed chitosans for wound dressings. *Carbohydrate Polymers*, *55*(1), 65-76. doi:10.1016/j.carbpol.2003.08.004

Loh, Q. L., & Choong, C. (2013). Three-dimensional scaffolds for tissue engineering applications: role of porosity and pore size. *Tissue Engineering Part B: Reviews*, 19(6), 485-502. doi:10.1089/ten.teb.2012.0437

Lu, Q., Zhang, B., Li, M., Zuo, B., Kaplan, D. L., Huang, Y., & Zhu, H. (2011). Degradation mechanism and control of silk fibroin. *Biomacromolecules*, *12*(4), 1080-1086. doi:10.1021/bm101422j

MacNeil, S. (2007). Progress and opportunities for tissue-engineered skin. *Nature*, *445*(7130), 874-880. doi:10.1038/nature05664

Mirahmadi, F., Tafazzoli-Shadpour, M., Shokrgozar, M. A., & Bonakdar, S. (2013). Enhanced mechanical properties of thermosensitive chitosan hydrogel by silk fibers for cartilage tissue engineering. *Materials Science and Engineering: C*, *33*(8), 4786-4794. doi:10.1016/j.msec.2013.07.043

Nelson, D. L., & Cox, M. M. (2013). *Lehninger Principles of Biochemistry* (Y. M. Elçin, Ed. & Trans. from 5th Ed.). Palme. (Original work published 2008).

Pamuk, F. (2011). *Biyokimya*. Gazi Kitabevi.

Park, D. H., Choi, W. S., Yoon, S. H., Shim, J. S., & Song, C. H. (2007). A developmental study of artificial skin using the alginate dermal substrate. *Key Engineering Materials*, *342-343*, 125-128. doi:10.4028/www.scientific.net/KEM.342-343.125

Peretz, S. (2004). Interaction of alginate with metal ions, cationic surfactants and cationic dyes. *Rom. Journal. Phys.*, *49*(9-10), 857-865.

Porter, D., & Vollrath, F. (2009). Silk as a biomimetic ideal for structural polymers. *Advanced Materials*, *21*(4), 487-492. doi:10.1002/adma.200801332

Priya, S. G., Jungvid, H., & Kumar, A. (2008). Skin tissue engineering for tissue repair and regeneration. *Tissue Engineering Part B: Reviews*, *14*(1), 105-118. doi:10.1089/teb.2007.0318

Qi, Y., Wang, H., Wei, K., Yang, Y., Zheng, R.-Y., Kim, I. S., & Zhang, K.-Q. (2017). A review of structure construction of silk fibroin biomaterials from single structures to multi-level structures. *International Journal of Molecular Sciences*, *18*(3), 237. doi:10.3390/ijms18030237

Reinholz, G. G., Lu, L., Saris, D. B. F., Yaszemski, M. J., & O'Driscoll, S. W. (2004). Animal models for cartilage reconstruction. *Biomaterials*, *25*(9), 1511-1521. doi:10.1016/S0142-9612(03)00498-8

Rujiravanit, R., Kruaykitanon, S., Jamieson, A. M., & Tokura, S. (2003). Preparation of crosslinked chitosan/silk fibroin blend films for drug delivery system. *Macromolecular Bioscience*, *3*(10), 604-611. doi:10.1002/mabi.200300027

Shen, Y., Wang, X., Li, B., Guo, Y., & Dong, K. (2022). Development of silk fibroin-sodium alginate scaffold loaded silk fibroin nanoparticles for hemostasis and cell adhesion. *International Journal of Biological Macromolecules*, *211*, 514-523. doi:10.1016/j.ijbiomac.2022.05.064

Sittinger, M., Bujia, J., Rotter, N., Reitzel, D., Minuth, W. W., & Burmester, G. R. (1996). Tissue engineering and autologous transplant formation: practical approaches with resorbable biomaterials and new cell culture techniques. *Biomaterials*, *17*(3), 237-242. doi:10.1016/0142-9612(96)85561-X

Summer, G. J., Puntillo, K. A., Miaskowski, C., Green, P. G., & Levine, J. D. (2007). Burn injury pain: the continuing challenge. *The Journal of Pain*, *8*(7), 533-548. doi:10.1016/j.jpain.2007.02.426

Toon, M. H., Maybauer, D. M., Arceneaux, L. L., Fraser, J. F., Meyer, W., Runge, A., & Maybauer, M. O. (2011). Children with burn injuries-assessment of trauma, neglect, violence and abuse. *Journal of Injury & Violence Research*, *3*(2), 98-110. doi:10.5249/jivr.v3i2.91

Um, I. C., Kweon, H., Park, Y. H., & Hudson, S. (2001). Structural characteristics and properties of the regenerated silk fibroin prepared from formic acid. *International Journal of Biological Macromolecules*, *29*(2), 91-97. doi:10.1016/S0141-8130(01)00159-3

Vepari, C., & Kaplan, D. L. (2007). Silk as a biomaterial. *Progress in Polymer Science*, *32*(8-9), 991-1007. doi:10.1016/j.progpolymsci.2007.05.013

Wang, X., Partlow, B., Liu, J., Zheng, Z., Su, B., Wang, Y., & Kaplan, D. L. (2015). Injectable silk-polyethylene glycol hydrogels. *Acta Biomaterialia*, *12*, 51-61. doi:10.1016/j.actbio.2014.10.027

Woo, W.-M. (2019). Skin Structure and Biology. In: C. Xu, X. Wang, & M. Pramanik (Eds.) *Imaging Technologies and Transdermal Delivery in Skin Disorders* (pp. 1-14). Wiley. doi:10.1002/9783527814633.ch1

Xie, H., Bai, Q., Kong, F., Li, Y., Zha, X., Zhang, L., Zhao, Y., Gao, S., Li, P., & Jiang, Q. (2022). Allantoin-functionalized silk fibroin/sodium alginate transparent scaffold for cutaneous wound healing. *International Journal of Biological Macromolecules*, *207*, 859-872. doi:10.1016/j.ijbiomac.2022.03.147

Yodmuang, S., McNamara, S. L., Nover, A. B., Mandal, B. B., Agarwal, M., Kelly, T.-A. N., Chao, P.-h. G., Hung, C., Kaplan, D. L., & Vunjak-Novakovic, G. (2015). Silk microfiber-reinforced silk hydrogel composites for functional cartilage tissue repair. *Acta Biomaterialia*, *11*, 27-36. doi:10.1016/j.actbio.2014.09.032

Yu, J. R., Navarro, J., Coburn, J. C., Mahadik, B., Molnar, J., Holmes IV, J. H., Nam, A. J., & Fisher, J. P. (2019). Current and future perspectives on skin tissue engineering: key features of biomedical research, translational assessment, and clinical application. *Advanced Healthcare Materials*, *8*(5), 1801471. doi:10.1002/adhm.201801471

Zhang, K. H., & Mo, X. M. (2011). Influence of Post-treatment with Methanol Vapor on the Properties of SF/P (LLA-CL) Nanofibrous Scaffolds. *Advanced Materials Research*, *236-238*, 2221-2224. doi:10.4028/www.scientific.net/AMR.236-238.2221

Zhang, T., Xiong, Q., Shan, Y., Zhang, F., & Lu, S. (2021). Porous Silk Scaffold Derived from Formic Acid: Characterization and Biocompatibility. *Advances in Materials Science and Engineering*, *2021*, 3245587. doi:10.1155/2021/3245587

Zhao, M., Qi, Z., Tao, X., Newkirk, C., Hu, X., & Lu, S. (2021). Chemical, thermal, time, and enzymatic stability of silk materials with silk i structure. *International Journal of Molecular Sciences*, *22*(8), 4136. doi:10.3390/ijms22084136